IEEE Access
Multidisciplinary ⋮ Rapid Review ⋮ Open Access Journal

Received December 8, 2021, accepted December 23, 2021, date of publication December 30, 2021,
date of current version January 7, 2022.

Digital Object Identifier 10.1109/ACCESS.2021.3139451

Numerical Analysis of Users' Body Effects on a Fourteen-Element Dual-Band 5G MIMO Mobile Terminal Antenna

AHMED MOHAMED ELSHIRKASI[1], AZREMI ABDULLAH AL-HADI[1], (Senior Member, IEEE), RIZWAN KHAN[2], PRAYOOT AKKARAEKTHALIN[3], (Member, IEEE), HAITHAM S. BEN ABDELMULA[4], AHMED M. BELGHASEM[5], AKRAM H. JEBRIL[6,7], AND PING JACK SOH[1,8], (Senior Member, IEEE)

[1]Advanced Communication Engineering (ACE) Center of Excellence, School of Computer and Communication Engineering, Universiti Malaysia Perlis, Kangar, Perlis 01000, Malaysia
[2]Department of Research and Development, Laird Technologies (M) Sdn Bhd, Perai, Penang 13600, Malaysia
[3]Department of Electrical and Computer Engineering, Faculty of Engineering, King Mongkut's University of Technology North Bangkok (KMUTNB), Bangsue, Bangkok 10800, Thailand
[4]College of Computer Technology Zawia, Ministry for Technical & Vocational Education, Tripoli, Libya
[5]College of Renewable Energies Tajoura, Ministry for Technical & Vocational Education, Tripoli, Libya
[6]Faculty of Engineering, School of Electrical Engineering, Universiti Teknologi Malaysia (UTM), Johor Bahru, Johor 81310, Malaysia
[7]Department of Communication Engineering, Technical College of Civil Aviation and Meteorology, Esbea, Tripoli 84116, Libya
[8]Centre for Wireless Communications (CWC), University of Oulu, 90570 Oulu, Finland

Corresponding authors: Azremi Abdullah Al-Hadi (azremi@unimap.edu.my) and Prayoot Akkaraekthalin (prayoot.a@eng.kmutnb.ac.th)

This work was supported in part by the Fundamental Research Grant Scheme (FRGS) through the Ministry of Education Malaysia under Grant FRGS/1/2019/TK04/UNIMAP/02/21, and in part by the King Mongkut's University of Technology North Bangkok under Grant KMUTNB-FF-65-21. The work of Ping Jack Soh was supported by the Academy of Finland 6Genesis Flagship under Grant 318927.

ABSTRACT This paper studies the performance of a 14-element dual-band 5G MIMO antenna with body effect and an antenna selection. The antenna operates in the lower frequency band from 3.10 to 3.85 GHz for 5G bands of LTE 42 and 43, whereas the upper band is from 5.60 to 7.20 GHz for the newly assigned 6 GHz WiFi band. The antenna performance was evaluated in free space and under the effect of human body in three scenarios, namely one-hand, two-hands, and call mode. All resulting envelope correlation coefficients are less than 0.3. On the other hand, the free space efficiency of the antenna elements is between 41 % to 77 % in the lower band and 61 % to 95 % in the upper band. Meanwhile, the efficiency of the elements varies depending on the interaction between each element with the hands and the head, with the least obstructed element efficiency degrading to 8 % relative to free space levels. Due to the body effect, multiplexing efficiency loss varies from 2.68 dB to 5.93 dB and the capacity loss is from 14 % to 38 %. Finally, a selection algorithm is used to assess the performance of the overall antenna when 12, 10 and 8 antenna elements are selected for operation. In free space and with number of elements 12, 10 and 8, the system achieves 91.7 %, 80 % and 67 % from the capacity of the 14-element MIMO antenna, respectively. However, in the vicinity of the body, these values increase to 96.3 %, 85.0 % and 72 % from the capacity of the 14-element MIMO antenna, respectively. This signifies that the less-contributing elements as a result of body blockage can be deselected in order to preserve system resources that these elements consume while contributing less significantly to the performance.

INDEX TERMS Multiple-input-multiple-output antennas, antenna selection, channel capacity, user effects.

I. INTRODUCTION

Multiple input multiple output (MIMO) antennas are deployed on both sides of the wireless communication link to achieve higher performance over single input single output (SISO) antennas without demanding higher bandwidth or transmit power [1]. Key advantages of MIMO antennas are multiplexing, beamforming, and spatial diversity to increase data rates, improving link reliability and achieve protection against interference [2], [3].

The associate editor coordinating the review of this manuscript and approving it for publication was Luyu Zhao.

In the 3G and 4G mobile communication systems, the number of MIMO antenna elements on a mobile terminal was between two and four elements. This number of elements is adequate to fulfill the performance requirements of these systems [4]. However, in 5G systems, more antenna elements are required on the mobile terminal to achieve the higher performance envisioned [5]. Nevertheless, the higher number of antenna elements on the mobile terminal requires more circuitry and signal processing [6]. Furthermore, the limited space on the chassis may restrict the number of elements that can be installed. Researchers have proposed 5G MIMO antennas for mobile terminals with different number of elements and different operating frequency bands. For instance, [7]–[10] proposed 8-element MIMO antennas for 5G mobile terminals, a 10-element MIMO antennas in [11]–[13], a 12-element MIMO antenna in [4] and [14], 14-element and 16-element MIMO antennas in [15] and [16], respectively. Even as high as 20-element MIMO antenna was proposed in [17]. However, in practice, the performance of MIMO antennas on mobile terminals is limited by aspects such as the human body's effect. This effect eventually will result in a major degradation in the link-level performance of the wireless system [18]. Therefore, the human body needs to be considered when evaluating the performance of MIMO antennas of mobile, and consequently, techniques to alleviate this effect need to be proposed [19]–[21].

In this paper, a 14-element MIMO antenna for 5G applications is proposed. The performance of the antenna is evaluated in free space and when the device is used in the vicinity of human body in three interaction scenarios – one-hand grip, two-hand grip, and call mode. Different metrics are used to evaluate the antenna performance in the multipath propagation environment.

Finally, an algorithm for antenna selection and removal of elements with least contribution is used to evaluate antenna capacity when the device is used in free space and under the three scenarios of interaction with the human body. This work's contribution is the application of the antenna selection algorithm, in addition to the performance evaluation of the antenna in various interactions scenarios with the user's body. This is done to identify and exclude low-contribution antenna elements caused by body blockage, thereby saving system resources that these elements would otherwise consume.

The organization of the paper is as follows. The next section presents the antenna details and the selected scenarios of interaction with the human body. Then, the radiation performance of the antenna is discussed in the following section in terms of S-parameters, radiation pattern, efficiency and specific absorption rate. Section 4 then presents the envelope correlation coefficient (ECC) results, followed by the multiplexing efficiency and ergodic capacity results in sections 5 and 6, respectively. Section 7 presents the antenna capacity results when the antenna selection algorithm is applied, before the conclusion is presented in section 8.

II. MIMO ANTENNA DESIGN

Fig. 1 shows the geometry of the proposed 14-element MIMO antenna integrated on a mobile terminal chassis. All antenna dimensions (length and height) are reasonably selected for practical mobile phones. The proposed antenna consists of a monopole with two branches, and is placed on a metallic ground plane sized at 160 mm × 80 mm × 0.3 mm. The antenna is fed from the first L-shaped arm using a discrete port. Two unequal monopole arm lengths are stacked on top of each other and optimized to obtain a dual band characteristic. The longer monopole branch is designed to operate in the lower 5G frequency band, whereas the shortest branch for operation in the whole 6-GHz WiFi band. The thickness of the metal is same for the whole monopole. The orientation of the antennas is also optimized to get better reflection coefficient and isolation.

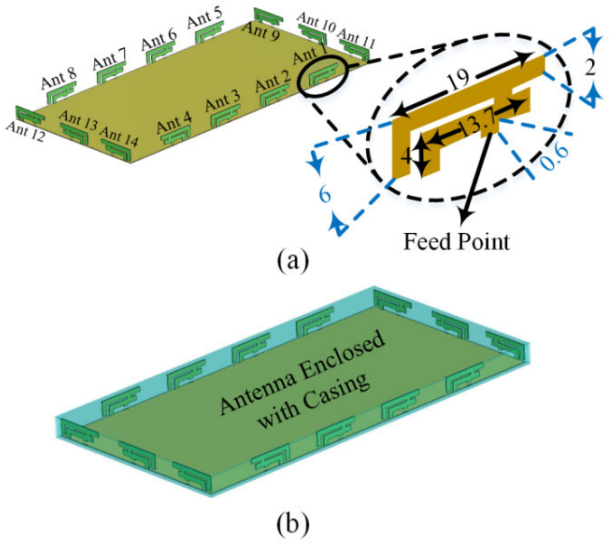

FIGURE 1. (a) Antenna elements on the chassis with the dimensions of the element (in mm). (b) The antenna enclosed casing.

As mobile terminals are mostly used in the vicinity of human body, the proposed antenna performance is evaluated in the vicinity of the human body in three situations – one-hand grip, tow-hand grip and finally in the call mode. Human body phantoms in the CST software are used to evaluate the performance of these three interactions, as shown Fig. 2.

III. RADIATION PERFORMANCE

A. S PARAMETERS

Fig. 3 shows the S-parameters of the antennas in operating bands. The lower band (LB) has a frequency bandwidth of 0.75 GHz from 3.10 to 3.85 GHz. This range includes the 5G bands of LTE 42 and 43, from 3.4 to 3.8 GHz [22]. The far-field radiation patterns of the antenna elements in this band are simulated every 50 MHz, resulting in 16 frequency points for every scenario among the four investigated scenarios (one free space and three scenarios with the human body). In addition to that, the upper band (UB) covers a wider

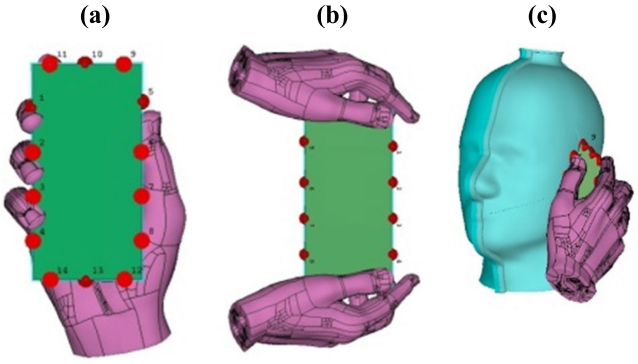

FIGURE 2. Scenarios of the performance evaluation under interaction with human body. (a) One hand. (b) Two hands. (c) Call mode.

frequency bandwidth of 1.6 GHz from 5.60 GHz to 7.20 GHz. This range contains the newly allocated 6-GHz WiFi band, operating from 5.925 to 7.125 GHz. This WiFi band was expanded by the Federal Communications Commission to meet the growing bandwidth demands of WiFi channels [23]. The far-field radiation patterns of the antenna elements are simulated every 100 MHz (with total of 18 frequency points) in each evaluation scenario.

B. FAR-FIELD RADIATION PATTERN

The far-field radiation patterns of four selected antenna elements (elements 2, 6, 10 and 13) in the x-y plane are shown in Fig. 4 at 3.5 GHz (LB). The radiation pattern is simulated in free space and when the device is used in the vicinity of the human body for the three cases. The selected antenna elements are located on each of the four sides of the chassis. Due to this, the effects of the human body for the three on-body cases is noticeable, as the radiation pattern of elements are in direct contact with the hand and/or the head. For instance, elements 2 and 6 are obstructed in the one-hand scenario, thus their radiation patterns are more distorted compared to the other two antenna elements which are further away in this scenario. On the contrary, the patterns for elements 10 and 13 are obstructed by the two-hand grip compared to elements 2 and 6. Finally, the performance of the elements in the call mode is similar to the one-hand case, with more deterioration. However, detailed quantitative results of interaction effect between the human body and each antenna element will be discussed in the next section.

In addition, the 3D realized gain of the same antenna elements which are 2, 6, 10, 13 in free space are shown in Fig. 5.

C. EFFICIENCY

The efficiency of the 14 antenna elements in both bands (in free space and the three on-body cases) is illustrated in Fig. 6. In free space, all elements show similar efficiency in terms of values and increase/decrease behavior with frequency. Another observation is that the efficiency of the antenna elements is higher in the UB than in the LB. The free space

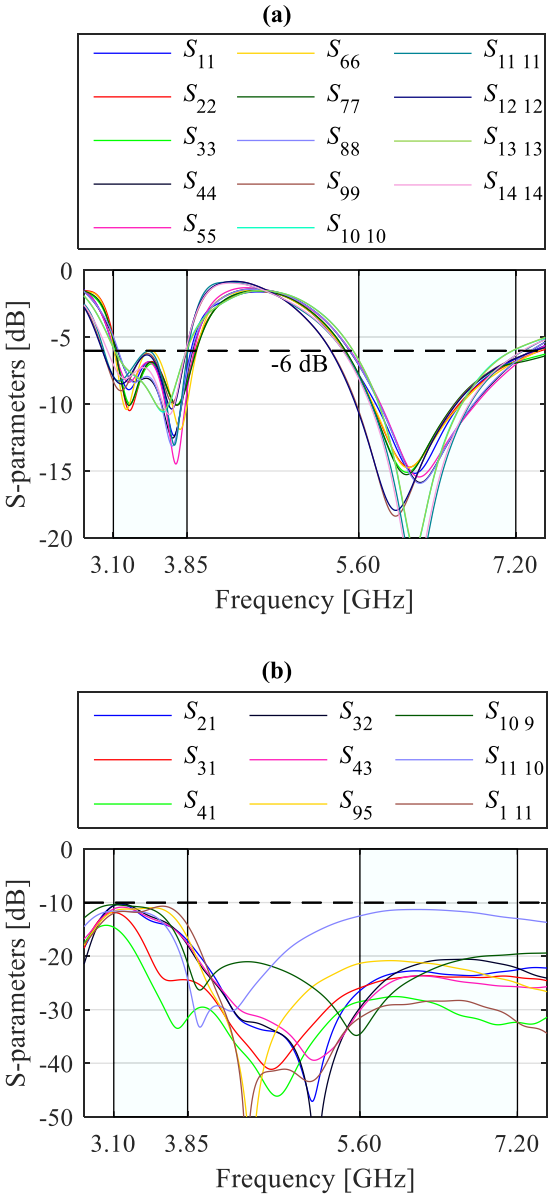

FIGURE 3. S-parameters of the antennas in free space. (a) Reflection coefficient. (b) Isolation.

efficiency in the LB ranges from 41 % to 77 %, whereas the performance is higher in the UB with values from 61 % up to 95 %. On the contrary, the efficiency of each antenna element in the vicinity of the human body varies depending on the interaction between the element and the hands and/or the head. When the device is held by one hand, the elements on the long sides of the chassis are more affected by the hand, whereas the elements on the short sides of the chassis remained free. Therefore, efficiencies of obstructed elements degraded severely, whereas the unobstructed elements maintained higher efficiencies. In the LB, the best performing antenna is element 9 with an efficiency ranging from 33 % to 55 %. On the other hand, the most affected antenna is element number 6, which efficiency dropped to values between 10 % and 28 %. Meanwhile, in the UB, elements 5 and 9 preserved

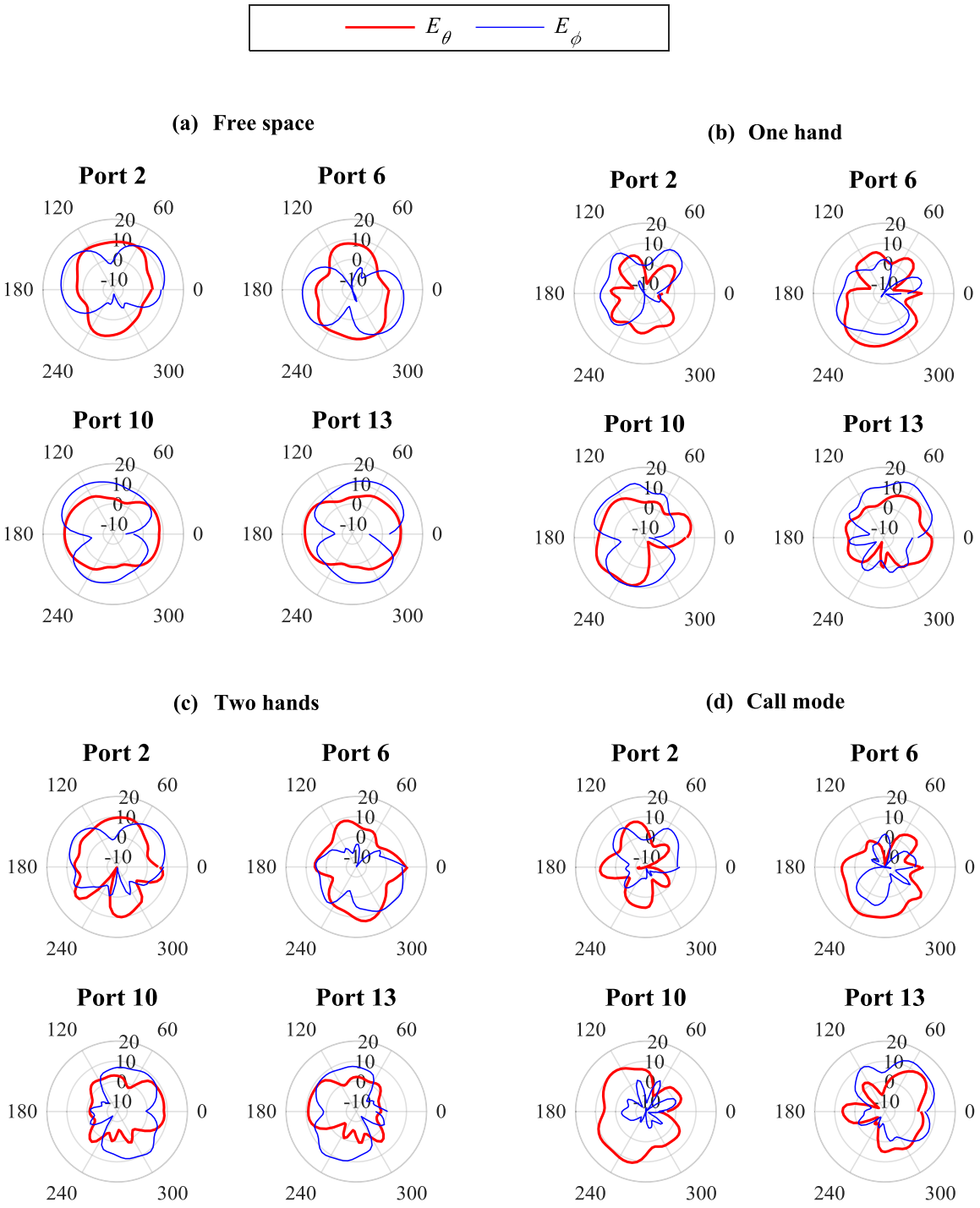

FIGURE 4. Far-field radiation pattern of four selected elements in the x-y plane for both horizontal polarization component (E_θ) and vertical polarization component (E_ϕ). (a) In free space. (b) One-hand grip. (c) Two-hand grip. (d) Call mode.

their performance, producing the highest efficiency between 55 % and 74 %, whereas element 3 showed the low efficiency from 14 % to 27 %.

An important observation is on the higher efficiency of element 11, which is located on the top side of the chassis. The index finger placed behind this element caused degraded its efficiency to be the smallest among elements on the short sides of the chassis. The efficiency of element 11 is from 19 % to 34 % in the LB and around 25 % in the UB.

Next, the antenna interaction when the device is held by the two hands is studied. Generally, in this case the elements located on the short sides of the chassis are covered by

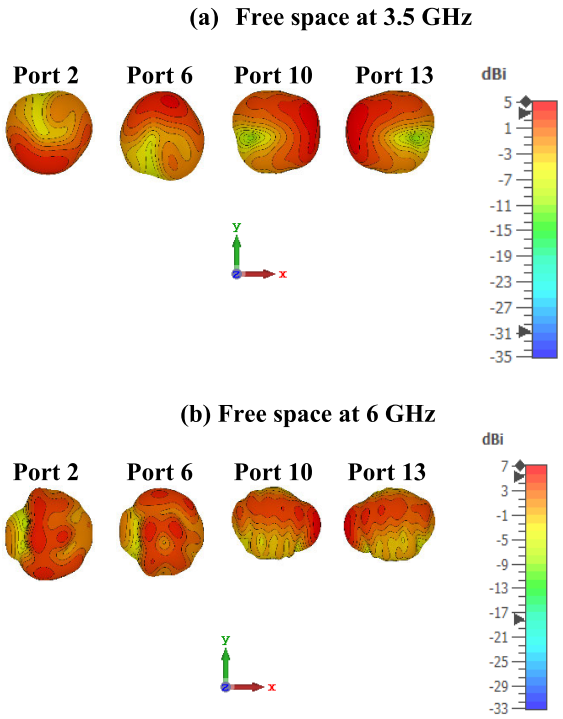

FIGURE 5. 3D realized gain of the antenna elements 2, 6, 10 and 13 in free space. (a) at 3.5 GHz and (b) at 6 GHz.

hands, whereas elements on the long sides are free. Thus, the efficiency behavior of elements when the chassis is held using the two-hand grip is the opposite to the performance of the one-hand grip. With the former, the highest efficiency in the LB is seen on elements 2, 3, 6, 7, and the efficiency of these elements increases with frequency from 30 % to 64 %. On the contrary, the most affected elements in the LB with the two-hand grip are 9 and 12, with severe efficiency degradation ranging from 12 % to 29%. Furthermore, the efficiency of elements under the two-hand grip on the UB behaves similarly with the LB in this interaction scenario. Elements 1, 2, 3, 6, 7 sustained the highest efficiencies, from 60 % to 78 %, while the least efficiency is produced by the obstructed elements 9 and 12 with efficiency between 17 % and 20 %.

Finally, the third interaction scenario with the body is when the device is evaluated in the call mode. Due to the direct contact between the antenna elements and the larger body tissue mass from hand and head, the resulting performance in this case is the worst. Similar to the one-hand scenario performance, the elements on the long sides of the chassis deteriorated more severely compared to the elements on the short sides of the chassis. In the LB, all elements exhibited similar efficiency, with a maximum efficiency of 30 % shown by element 9, and the worst efficiency of 8% by element 12. Despite not being obstructed by the hand, the low performance of element 12 is caused by the direct contact with the head. On the other hand, the efficiency in the UB is up to 51 % produced by element 9, and is as low as 10 % seen by element 6.

The results from this section showed that up to 14 antenna elements can be placed on the chassis with satisfactory performance in free space. However, the interaction with human hands and head is unavoidable and resulted in the efficiency degradation, depending on the scenario of interaction. This fact must be considered to ensure that the high number of elements will improve the performance of MIMO antennas in practice. One of the methods alleviate the effects of blockage is by applying antenna selection algorithms aimed at reducing resources consumed by the obstructed elements and maximizing the contribution of the unobstructed elements to optimize the overall system performance.

D. SPECIFIC ABSORPTION RATE (SAR)

The Specific Absorption Rate (SAR) is the amount of electromagnetic energy absorbed by a human body and is measured in watts per kilogram (W/kg). To ensure that a wireless communications device meets the requirements for radio frequency (RF) exposure, wireless devices with radiating parts that are close to the human body must undergo SAR testing [24]. In this work, we show SAR analysis for only call mode where the mobile phone is close to the human head and if the SAR exceeds the maximum limit inside the head, it causes health hazards to the human brain. The maximum SAR over 10g of tissue is 1.92 W/kg. This value is below the maximum allowed value of 2.0 W/kg over 10g [25]. SAR results show that the proposed antenna is safe to use in its call mode. The SAR values at 3.5 GHz and 6 GHz are shown in Fig. 7 at frequencies of 3.5 GHz and 6 GHz.

IV. ENVELOPE CORRELATION COEFFICIENT

Envelope correlation coefficient (ECC) between two antennas characterizes how independent are their far-field radiation patterns. ECC is calculated from the relation given in [26]. Ideally, two independent antennas will have null ECC, whereas a set of fully correlated antennas have ECC of unity. For an acceptable MIMO antenna performance in practical systems, ECC value should be less than 0.5 [27] and this value was revised to be below 0.3 in 4G systems [28]. However, the work in [29] showed that ECC is highly dependent the distribution of the propagation environment. More specifically, the ECC values below these two thresholds in the uniform environment can be higher when narrow beam incident waves are considered. Assuming a uniform environment, ECC is evaluated as follows [26]:

$$ECC = \frac{\left|\iint_{4\pi} E_1(\theta,\phi) * E_2(\theta,\phi)\, d\Omega\right|^2}{\iint_{4\pi} |E_1(\theta,\phi)|^2\, d\Omega \iint_{4\pi} |E_2(\theta,\phi)|^2\, d\Omega} \quad (1)$$

where $E_i(\theta,\phi)$ denotes the ith antenna's complex three-dimensional (3-D) radiated far-field pattern.

The number of ECC values of an n-element MIMO antenna is $n(n-1)/2$ at every frequency point (simulated or measured). Thus, for the 14-port MIMO antenna proposed in his

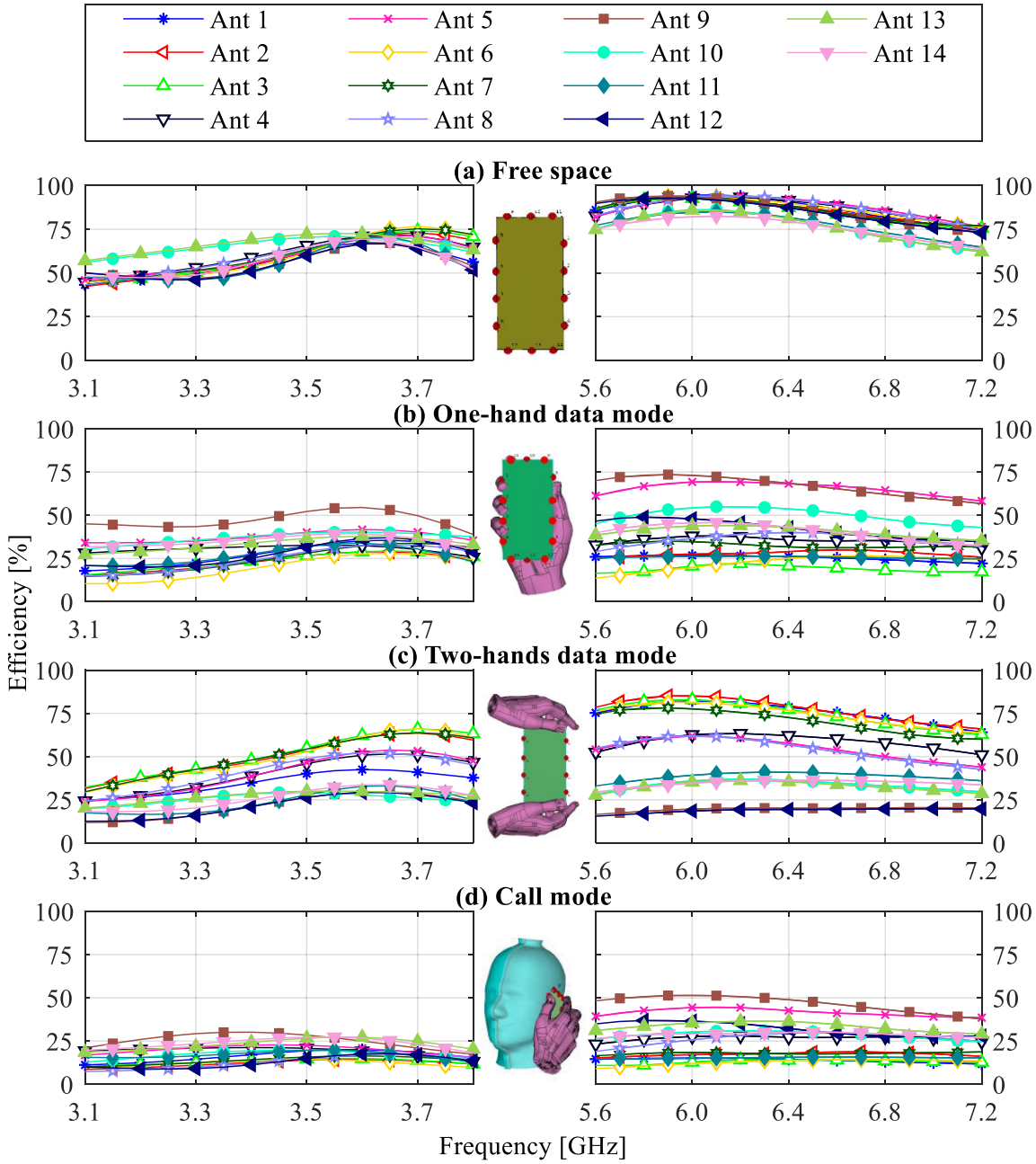

FIGURE 6. Efficiency of the 14 elements. (a) Free space. (b) One-hand grip. (c) Two-hand grip. (d) Call mode.

work, there will be 91 values at every simulation frequency point. For brevity reasons, ECC curves are omitted from this work. Instead, the maximum ECC values in the lower and higher bands in free space and with the different interaction scenarios with the human body will be reported. Table 1 summarizes these maximum ECC values assuming a uniformly distributed incident signal. In both frequency bands the ECC is below the 0.3 threshold. Furthermore, ECC values in the LB are higher than in UB, due to LB's longer wavelengths with the same physical distance. Hence, the separation distance in terms of wavelength between antenna elements become shorter in the LB. On the other hand, ECC increases when the device is used in the vicinity of the human body, with the highest ECC produced when the device is used in call mode in both bands. These ECC values indicate that up to 14 antenna elements can be integrated onto a common mobile terminal to operate in both frequency bands with acceptable ECC performance.

V. MULTIPLEXING EFFICIENCY

Multiplexing efficiency (η_{mux}) is a parameter related to the signal to noise power ratio (SNR) of MIMO antennas on

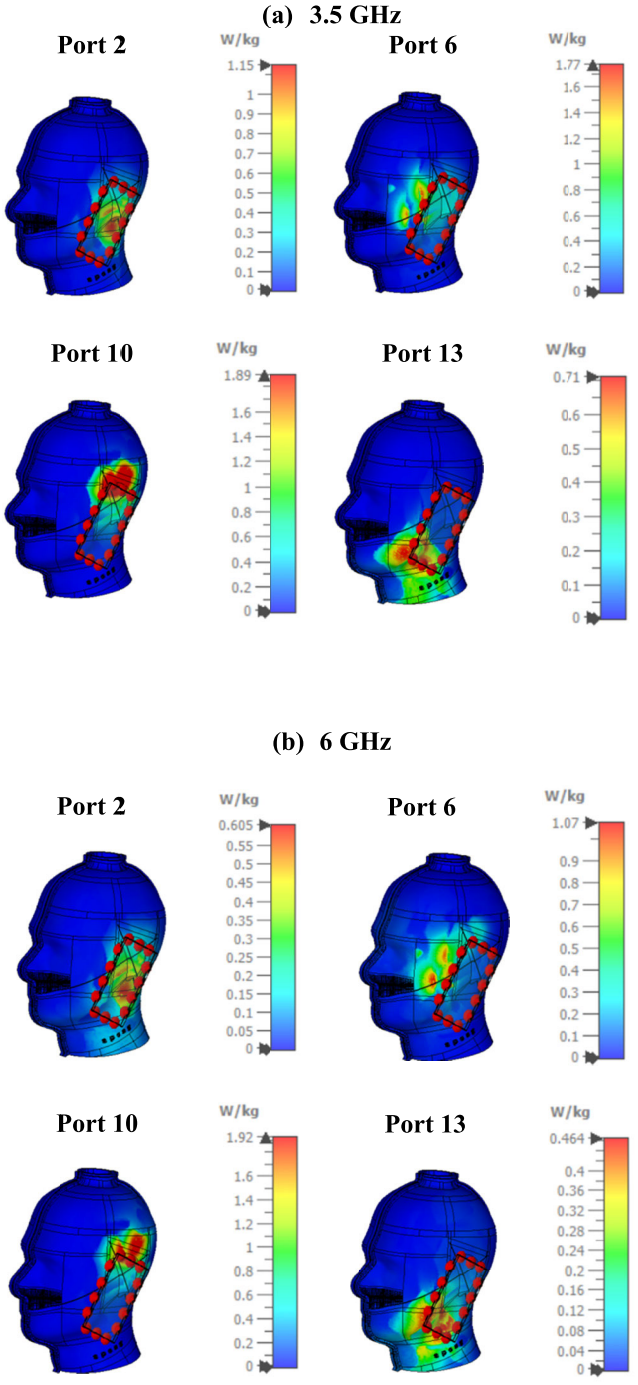

FIGURE 7. SAR values of antenna elements 2, 6, 10 and 13 at (a) 3.5 GHz, (b) 6GHz.

mobile terminals. It is defined as the quotient of the SNR of the MIMO antenna under test (SNR_{AUT}) to the SNR of an ideal MIMO antenna system (SNR_{IID}). The ideal SNR is obtained from an independent and identically distributed (IID) MIMO antenna. Both of antennas are assumed to have the same number of elements, and they achieve the same ergodic capacity at these SNRs [30]. Fig. 8 illustrates the concept of the multiplexing efficiency.

TABLE 1. Maximum values of ECC of both bands in free space and in the vicinity of the human body.

Frequency band	Free space	One hand	Two hands	Call mode
LB	0.15	0.22	0.24	0.27
UB	0.02	0.10	0.08	0.14

Mathematically, η_{mux} is defined as:

$$\eta_{mux} = \frac{SNR_{IID}}{SNR_{AUT}} \tag{2}$$

or when both SNRs are in decibels (dB):

$$\eta_{mux}[\text{dB}] = SNR_{IID}[\text{dB}] - SNR_{AUT}[\text{dB}] \tag{3}$$

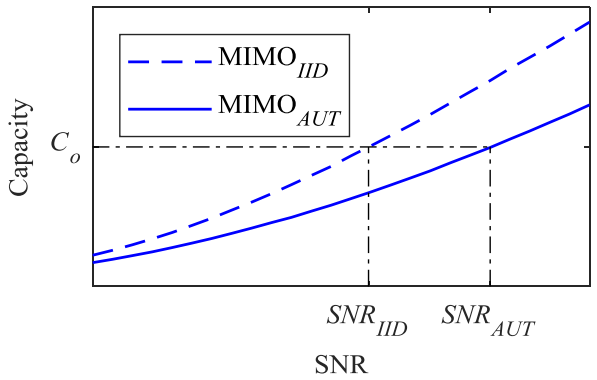

FIGURE 8. Concept of multiplexing efficiency, where both MIMO antennas have the same ergodic capacity at the respective SNRs.

η_{mux} can be calculated directly from the definition. However, this direct approach is computationally complex, and does not show a direct link between η_{mux} and the design metrics of the MIMO antenna (such as ECC and efficiency). Therefore, an approximate, closed-form η_{mux} formula was derived in [31] and used to evaluate the performance of MIMO mobile terminal antennas in [32]–[34], as follows:

$$\eta_{mux} = \sqrt[M]{\left(\prod_{i=1}^{M} \eta_i\right) \det(\bar{\boldsymbol{R}})} \tag{4}$$

where η_i is the efficiency of the i^{th} antenna element and $\det(\bar{\boldsymbol{R}})$ is the determinant of the complex correlation coefficient matrix $\bar{\boldsymbol{R}}$, which is constructed as follows [35]:

$$\bar{\boldsymbol{R}} = \begin{bmatrix} 1 & \rho_{c,12} & \cdots & \rho_{c,1M} \\ \rho_{c,12}^{*} & 1 & \cdots & \rho_{c,2M} \\ \vdots & \vdots & \ddots & \vdots \\ \rho_{c,1M}^{*} & \rho_{c,2M}^{*} & \cdots & 1 \end{bmatrix} \tag{5}$$

where $\rho_{c,ij}$ is the complex correlation coefficient between ports i and j, and $*$ is the conjugate operator. Besides the low computation complexity of η_{mux} from this closed-form equation, it consists of two main parts; a first part is $\sqrt[M]{\left(\prod_{i=1}^{M} \eta_i\right)}$ which the geometrical mean of individual efficiencies of

the antenna elements. The second part is $\sqrt[M]{\det(\bar{\boldsymbol{R}})}$ which depends on the correlation between antenna elements. This term gets close to 0 dB when all complex correlation coefficient between the AEs are close to 0. Optimizing these two parts enhances η_{mux} of the MIMO antenna.

Fig. 9 presents the multiplexing efficiency of the 14-element MIMO antenna in free space and in the three interaction scenarios with the human body. It observed that the contribution of the $\sqrt[M]{\det(\bar{\boldsymbol{R}})}$ term is insignificant in the deterioration of η_{mux} compared to the contribution from efficiency term. This is especially evident in the UB, where the ECC values are very low and resulting in a close-to-zero-dB $\sqrt[M]{\det(\bar{\boldsymbol{R}})}$ term. On the other hand, the drop in η_{mux} is caused mainly by the $\sqrt[M]{\left(\prod_{i=1}^{M}\eta_i\right)}$ term, which gets closer to the η_{mux} as the $\sqrt[M]{\det(\bar{\boldsymbol{R}})}$ term gets closer to 0 dB, especially in the UB.

The highest η_{mux} is seen when the antenna is operated in free space, where η_{mux} is between −4.07 dB and −2.17 dB in the LB, and from −1.46 dB to −0.42 dB in the UB. However, when the device is held by the user in different interaction scenarios, power is absorbed by the body tissues, hence deteriorating η_{mux}. In the one-hand mode, η_{mux} is reduced by around 3.05 dB and 3.81 dB in LB and UB, respectively compared to in free space. In the two-hand mode, the η_{mux} values are 2.77 dB and 2.68 dB below the free space levels in the LB and the UB, respectively. The highest η_{mux} loss is observed when the device is used in call mode, where the device is surrounded by more body tissues compared to the two previous interaction scenarios. The reduction in the η_{mux} in this case is around 5.93 dB in the LB and around 5.69 in the UB relative to free space.

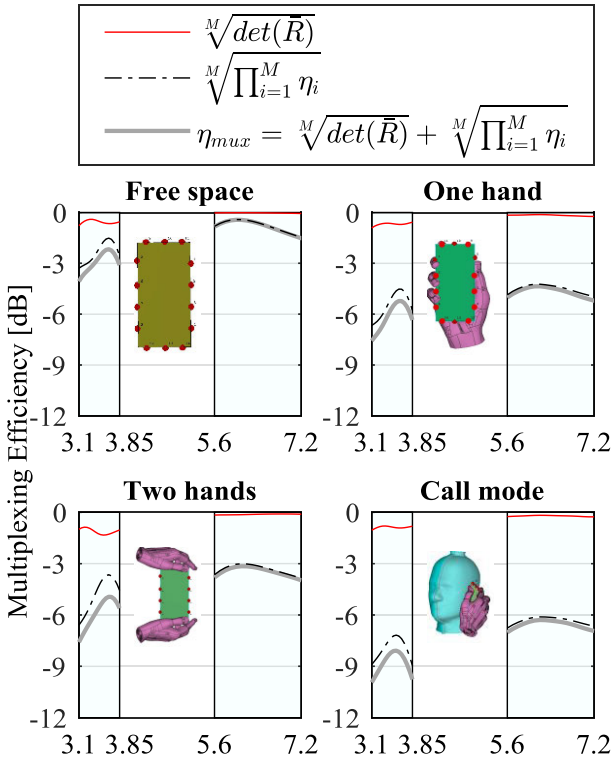

FIGURE 9. Multiplexing efficiency of the 14-element MIMO antenna, in free space and with the three interaction case with the human body.

VI. CAPACITY

Assuming that the channel state information (CSI) is available at the receiver only, and the transmitter power is allocated uniformly cross transmit antennas, MIMO capacity can be calculated from the following relation [36]:

$$c = E\left(log_2\left(det\left(I_{N_r} + \frac{SNR}{N_t}\boldsymbol{H}\boldsymbol{H}^{\dagger}\right)\right)\right) \tag{6}$$

where E is averaging operator, det is the determinant, I_{N_r} is the identity matrix of size N_r where N_r is the number of receive antenna elements, SNR is the signal to noise ratio, N_t is the number of transmit antenna elements, $\boldsymbol{H} \in C^{N_r \times N_t}$ is the wireless channel matrix, and $()^{\dagger}$ is the transpose of the complex conjugate.

The wireless channel matrix $\boldsymbol{H}$ in this work is constructed based on the model used in [37], [38]. The transmit side in this model assumes ideal antenna elements with 100 % efficiency and null ECC. In addition, the number of transmit antenna elements is fixed at 14 for all ergodic capacity calculations in this work. The wireless channel matrix $\boldsymbol{H}$ in this model is constructed as follows:

$$\boldsymbol{H} = \boldsymbol{R}^{1/2}\boldsymbol{H}_{IID} \tag{7}$$

where $\boldsymbol{H}_{IID} \in \mathbb{C}^{N_r \times N_t}$ is the IID channel matrix which entries are complex and normally-distributed, with zero mean and unity variance specifically $CN(0, 1)$. This matrix models the uniform propagation environment between the transmitter and the receiver. $\boldsymbol{R} \in \mathbb{C}^{N_r \times N_r}$ is the receiver correlation matrix which involves the effects of the AUT, as follows:

$$\boldsymbol{R} = \boldsymbol{\Lambda}^{1/2}\bar{\boldsymbol{R}}\boldsymbol{\Lambda}^{1/2} \tag{8}$$

where $\boldsymbol{\Lambda}$ is the diagonal efficiency matrix written as:

$$\boldsymbol{\Lambda} = \begin{bmatrix} \eta_1 & 0 & \cdots & 0 \\ 0 & \eta_2 & \cdots & 0 \\ \vdots & \vdots & \ddots & \vdots \\ 0 & 0 & \cdots & \eta_{N_r} \end{bmatrix} \tag{9}$$

where η_i is the efficiency of the i^{th} antenna port, and $\bar{\boldsymbol{R}}$ is the complex correlation coefficient matrix in (5) of the multiplexing efficiency. Furthermore, all capacities are calculated by averaging 300,000 channel realizations at every frequency point to ensure their convergence to accurate values, considering the large number of antenna elements. In addition to that, all capacity results are obtained at the SNR value of 20 dB. Fig. 10 shows the ergodic capacity of the 14 × 14 MIMO antenna system in free space and in the three interaction scenarios with human body. In Fig. 10(a), the ergodic capacity performance is higher in the UB due to the higher efficiency of antenna elements and the lower ECC

in this band. Moreover, the capacity changes in frequency in both bands behave similarly with the efficiency levels of the elements presented in Fig. 6. This is another indication that the wireless channel model is mainly determined by the efficiency matrix $\mathbf{\Lambda}$, with significantly lower contribution from the complex ECC matrix $\bar{\boldsymbol{R}}$.

In free space, the LB capacity is between 60.6 and 68.3 bit/s/Hz, while the capacity in the UB is from 70.5 to 75.0 bit/s/Hz. The highest capacity value in the UB is 2 bit/s/Hz lower than the 14 × 14 IID capacity. Meanwhile, the capacity reduction of the antenna in the presence of the human body again depends on the interaction scenario between the antenna and the body. Again, the least capacity is obtained when the mobile is used in call mode. In one-hand grip and compared to the free space performance, the LB capacity is reduced by around 12 bit/s/Hz and UB capacity is lowered by around 15 bit/s/Hz. Next and compared to the free space, the two-hand grip capacity is decreased by around 11 bit/s/Hz in both bands, and finally in the call mode is decreased the most by about 22 bit/s/Hz in both bands. Fig. 10(b) illustrates the capacity loss resulting from the interaction with the human body in percentage, relative to the free space capacity. The one-hand grip causes capacity loss between 17 and 21 % in the LB, and around 21 % in the UB. Secondly, the two-hand grip reduces the capacity from 14 to 21 % relative to free space in the LB, and around 14% in the UB. Finally the highest loss observed is in the call mode, which ranges between 31 and 38 % in the LB and around 31 % in the UB.

Table 2 compares the performance of the proposed antenna array with various 5G MIMO handset antennas operating in the sub-6 GHz bands, ranging from 6 to 18 elements. It is evident from the table that the MIMO antenna performance degrades resulting from interactions with hands in various modes, as indicated by the ECC and efficiency. Furthermore, this table also highlights the number of antenna elements in each design which efficiency fell below 20 % due to severe hand blockage. Due to this, an antenna selection method is proposed to alleviate the issue of human body blockage, which will be explained in the following subsections. The following section suggests using an antenna selection to select antenna elements in good condition while excluding those that are severely obstructed by hand and head.

VII. ANTENNA SELECTION

The large number of antenna elements on the mobile terminal requires more system resources (RF circuitry, signal processing and channel estimation). Therefore, all antenna elements must effectively contribute to the system performance while consuming these resources. This section aims to understand how the different interaction scenarios between the antenna and human body can lower the contribution of selected elements in terms of capacity.

Finally, an antenna selection algorithm is used to optimize the overall contribution of these antenna elements in terms of capacity. In this section, the number of transmit

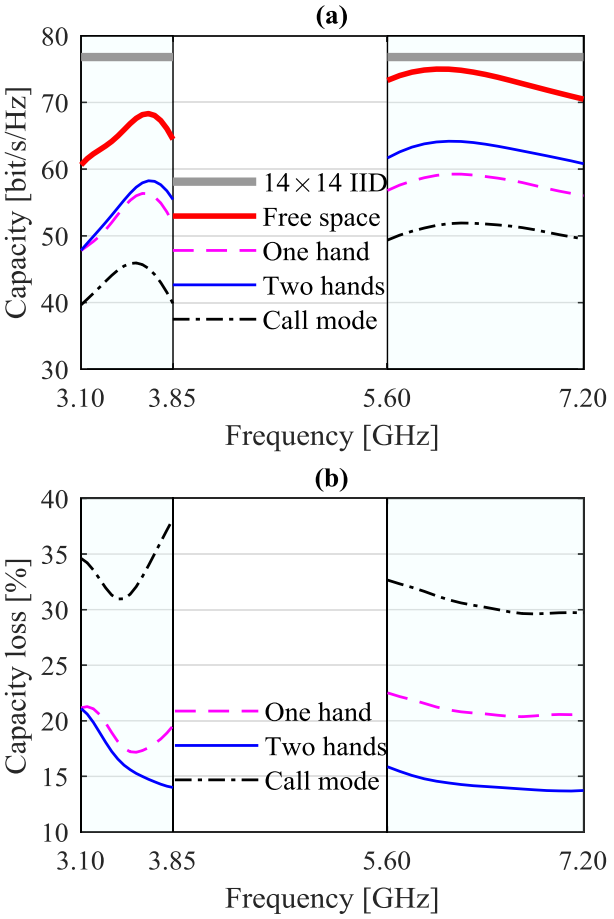

FIGURE 10. (a) Ergodic capacity of the 14-element MIMO antenna. (b) Ergodic capacity loss due to the interaction with the human body.

antennas N_t is fixed at 14, and on the receiver side L antennas are selected from the N_r available antennas on the mobile terminal. Furthermore, the wireless channel matrix with the antenna selection $\tilde{\boldsymbol{H}} \in \mathbb{C}^{L\times N_t}$ is constructed by selecting L rows from the available rows N_r in the channel matrix $\boldsymbol{H}$ of the full system. Hence, the set S which contains all possible different $\tilde{\boldsymbol{H}}$ matrices with L rows (i.e. L receive antennas) has a cardinality of M where $M = \binom{N_r}{L}$.

The optimal matrix $\tilde{\boldsymbol{H}}_{opt}$ must be selected among all possible M matrices in S to maximize the system capacity as follows [44]:

$$\tilde{\boldsymbol{H}}_{opt} = \underset{\tilde{\boldsymbol{H}}\in S}{agr\ max} \left\{ log_2 \left(det \left(I_L + \frac{SNR}{N_t} \tilde{\boldsymbol{H}} \tilde{\boldsymbol{H}}^{\dagger} \right) \right) \right\} \quad (10)$$

Selection of the $\tilde{\boldsymbol{H}}_{opt}$ can be conducted by an exhaustive search method, where the capacity from all possible M matrices in the set S is computed before the matrix with the highest capacity is selected. However, computing the capacities from all possible matrices in the set S is computationally complex and resource-consuming, especially with increasing number of antennas on the device. Therefore, several algorithms have been proposed to select the optimal $\tilde{\boldsymbol{H}}_{opt}$ with a balance of

TABLE 2. Performance comparison of different 5G antenna arrays.

References	Number of antenna elements	Frequency bands	type of interaction modes with body	ECC (free space)	Efficiency In free space	Maximum efficiency with body interaction	Number of elements with efficiency < 20% with body interaction
[39]	6	3.4 – 3.6 GHz	Data mode (one hand). Read mode (two hands).	< 0.30	45 – 57%	Data Mode: 54% Read Mode: 48%	-
[40]	8	Lower Band (LB): 3.4 – 3.6 GHz Upper Band (UB): 4.8 – 5.1 GHz	Right hand mode (RHM)	< 0.10	LB: 41 – 72%. UB: 40–85%.	LB: 60%. UB: 73%	2
[41]	10	Lower Band (LB): 3.4 – 3.8 GHz Upper Band (UB): 5.150 – 5.925 GHz	Data mode (one hand). Read mode (two hands).	< 0.15	LB: 42 – 65%. UB: 62 – 82%.	Data mode LB: 52%. UB: 68% Read mode LB: 58%. UB: 67%	Data mode LB: 4 UB: 3 Read mode LB: 2 UB:2
[4]	12	8 elements to operate on LTE bands 42/43 3.4 – 3.8 GHz 6 elements to operate on LTE band 46 5.150 –5.925 GHz	Right Hand Mode (RHM). Left Hand Mode (LHM). Read Mode (RM, two hands)	< 0.10	Bands 42/43: 41 – 82%. Band 46: 47 – 79%	Right Hand Mode LTE bands 42/43: 52%. LTE band 46: 60%. Left Hand Mode LTE bands 42/43: 55%. LTE band 46: 66%. Read Mode LTE bands 42/43: 53%. LTE band 46: 62%.	RHM LTE bands 42/43: 3 out of 8. LTE band 46: 3 out of 6. LHM LTE bands 42/43: 4 out of 8. LTE band 46: 4 out of 6. RM LTE bands 42/43: 2 out of 8. LTE band 46: 2 out of 6.
This work	14	Lower Band (LB): 3.10 – 3.85 GHz Upper Band (UB): 5.60 – 7.20 GHz	Data mode (one hand). Read mode (two hands). Call mode (hand and head)	< 0.15	LB: 41 – 77% UB: 61 – 95%	Data mode: LB: 55% UB: 74% Read mode: LB: 64% UB: 78% Call mode: LB: 30% UB: 51%	Data mode: LB: 3 UB: 2 Read mode: LB: 3 UB: 2 Call mode: LB: 8 UB: 6
[42]	16	5 – 6 GHz	Data mode (one hand)	< 0.31	51 – 76%	63%	5
[43]	18	LTE Bands 42/43 3.4 – 3.8 GHz	Data mode (one hand). Read mode (two hands).	< 0.10	87 – 93%	Data mode: 83%. Read mode: 86%	Data mode: 7 Read mode: 4

computational complexity and losses in performance [45]. Practical implementation of antenna selection algorithms can be hard when a set of switches is used to activate selected antennas only, or a soft selection can be implemented when all antennas are kept active and selection algorithm is implemented in the RF domain upon the received signals from all antennas [6]. In this work, an algorithm to select the L receive antennas on the mobile terminal (and consequently the optimal matrix $\tilde{\boldsymbol{H}}_{opt}$) is proposed based on the received power from each receive antenna. The i^{th} row in the full system channel $\boldsymbol{H}$ represents channel links from all transmitter antennas to the i^{th} receiver antenna. Thus, the *Frobenius* norm I is taken for each row as a measure of the received power through each receive antenna. Then, the L rows corresponding to the highest I values are selected to build the channel matrix $\tilde{\boldsymbol{H}}_{opt}$. The *Frobenius* norm I_i of the i^{th} row for $1 \leq i \leq N_r$ is calculated as follows [46]:

$$I_i = \sum_{j=1}^{N_t} \left\| h_{ij} \right\|^2 \tag{11}$$

where h_{ij} is the $(i,j)^{th}$ entry of the full system channel matrix $\boldsymbol{H}$.

The capacity with the antenna selection algorithm is presented in Fig. 11. Besides the 14 × 14 system capacity, the figure also shows the capacity of antenna selection

algorithm with three different L values of receive antennas (12, 10 and 8 elements). Results obtained in free space and under the influence of the human body in the three interaction scenarios are also presented.

When the two least-contributing elements are removed and the remaining 12 elements considered, the free space capacity is reduced by 5.4 bit/s/Hz in the LB and 6.2 bit/s/Hz in the UB compared to the full system capacity. Despite that, a smaller capacity reduction is observed with the 12 antenna elements when the device is used in the vicinity of human body. The capacity decreased from 2.3 to 2.7 bit/s/Hz below the full system capacity in both frequency bands and in the three cases of the interaction with the human body. Next, 10 antenna elements are selected to be evaluated. The capacity reduction in free space is from 12.4 to 14.5 bit/s/Hz in both frequency bands. On the other hand, there is less reduction observed when the device is used in the vicinity of the human body. The capacity declined by 6.8 to 8.7 bit/s/Hz in the three interaction cases over both frequency bands. Finally, when only 8 antenna elements are selected, the free space capacity is lowered by 20.8 to 24.2 bit/s/Hz in both bands. Moreover, the capacity in the vicinity of the human body declines by up to 12.0 bit/s/Hz in the call scenario and up to 16.8 bit/s/Hz when the device is held by two hands. It is seen that the excluded elements in all cases contributed minimally to the capacity when the device is used in the vicinity of human body compared to in the free space. This reduced contribution is due to the low performance of these excluded elements due to body blockage. However, note that the capacity drop in Fig. 11 is discussed as the difference in bit/s/Hz unit between the full system capacity and the capacity of different L-element system. This is without considering the peak values of the full MIMO antennas' capacity.

Fig. 12 shows the contribution of the L-element MIMO antenna in terms of capacity compared to the capacity of the full system. When $L = 12$, the free space capacity is up to 91.7 % relative to the 14-element free space capacity. This is then increased from 94.0 % to 96.3 % when the mobile terminal is evaluated in the vicinity of the human body for each case. Next, with $L = 10$, the system achieves up to 80 % of the 14-element antenna's free space capacity, whereas this increased to above 85 % in the vicinity of human body in the three different interaction scenarios. Lastly, the 8-element MIMO antenna's capacity achieved up to 67 % of the full system capacity in free space. This capacity then increased to above 72 % in the vicinity of the body.

From the results in Fig. 11 and Fig. 12, a selection algorithm can be applied to exclude less-contributing elements, especially when the device is used in the vicinity of the human body. This is to avoid the consumption of the system resources by these elements while they contribute less significantly in the performance. Therefore, exclusion of these elements enables the optimization of system resources with acceptable deterioration in the system capacity. On the other hand, the mobile terminal can be designed with extra antenna elements on the device, and the algorithm can periodically search for the best elements to be used especially when it is used in the vicinity of the human body.

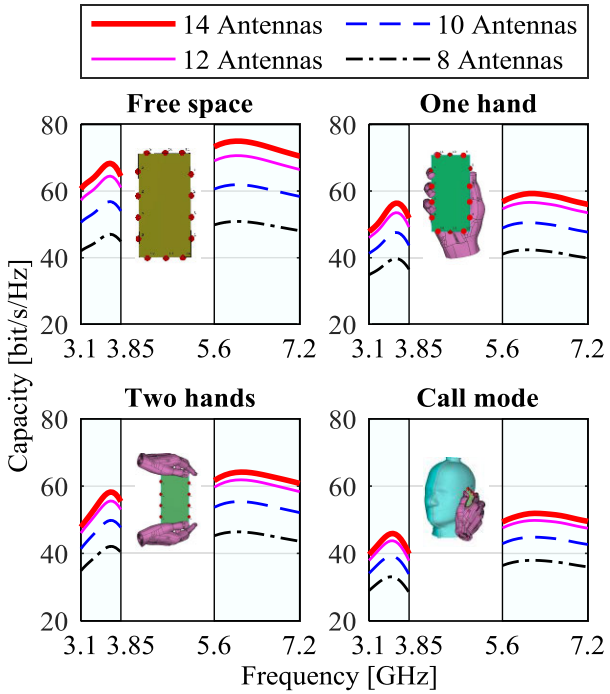

FIGURE 11. Capacity with 14, 12, 10 and 8 antenna elements selected in free space and the three interaction scenarios with the human body.

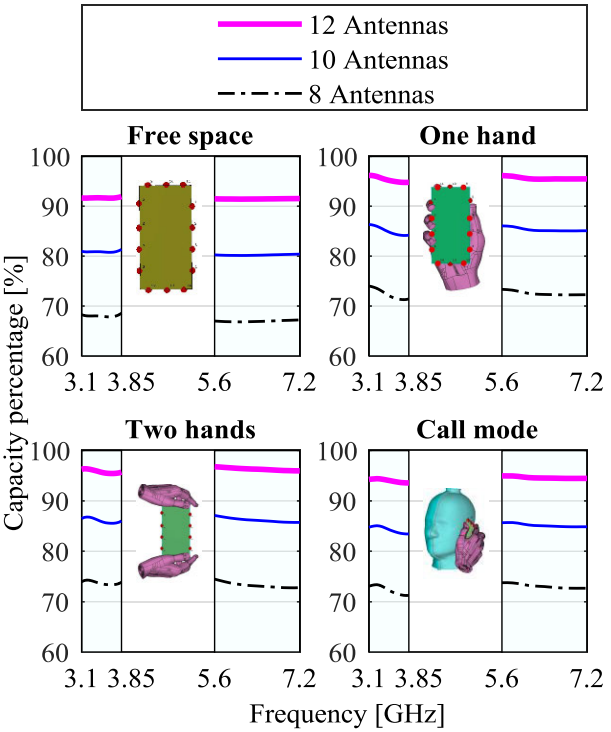

FIGURE 12. Contribution of the L-element system capacity in the 14-element system capacity; in free space and the three interaction scenarios with the human body.

It is understood from the results in the previous sections that the least-performing elements (which are excluded from

the channel matrix) change depending on the interaction scenarios with human body. Fig. 13 shows the probability of each element to be selected when 10 elements are considered. In free space, it is observed that all elements are equally likely to be selected due to the similar efficiency of antenna elements in free space, as shown in Fig. 6. However, when the device is used in the vicinity of the human body, the likelihood of an element being selected depends mainly on its interaction with the body, besides the quality of the propagation link of the particular channel realization.

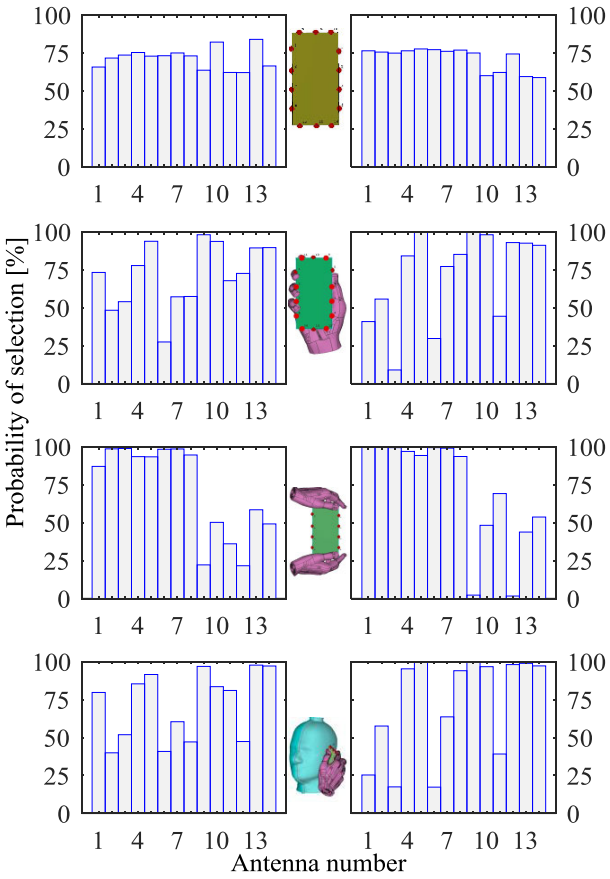

FIGURE 13. Probability of each antenna selection in free space and under the influence of the human body. (LB left, UB right).

VIII. CONCLUSION

This work presented a study on a 14-element MIMO antenna designed to operate for 5G applications. The antenna performance is first evaluated in free space before being assessed when used in three different near-human body cases. Despite maintaining the ECC values of less than 0.3 in all evaluation cases, the efficiency of the different antenna elements varies considerably, subjected to the type of interaction scenario with the body. The performance of the multiplexing efficiency and ergodic capacity showed that the antenna efficiency limitations are the main factor in the performance degradation. In addition to that, the antenna selection results indicated that the contribution of elements in the channel can be predicted from the antenna design stage. Further work is needed to further quantify the tradeoff between the contribution of antenna elements under the influence of the human body and the resources allocated to these elements.

REFERENCES

[1] K. Tiwari, D. S. Saini, and S. V. Bhooshan, "Antenna selection for MIMO systems over Weibull–Gamma fading channel," *Perspect. Sci.*, vol. 8, pp. 475–478, Sep. 2016.
[2] D. Astély, E. Dahlman, A. Furuskär, Y. Jading, M. Lindström, and S. Parkvall, "LTE: The evolution of mobile broadband," *IEEE Commun. Mag.*, vol. 47, no. 4, pp. 44–51, Jul. 2009.
[3] W. Fan, X. Carreño, P. Kyösti, J. Nielsen, and G. F. Pedersen, "Over-the-air testing of MIMO-capable terminals: Evaluation of multiple-antenna systems in realistic multipath propagation environments using an OTA method," *IEEE Veh. Technol. Mag.*, vol. 10, no. 2, pp. 38–46, Jun. 2015.
[4] Y. Li, C.-Y.-D. Sim, Y. Luo, and G. Yang, "12-Port 5G massive MIMO antenna array in sub-6 GHz mobile handset for LTE bands 42/43/46 applications," *IEEE Access*, vol. 6, pp. 344–354, 2017.
[5] M. S. Sharawi, M. Ikram, and A. Shamim, "A two concentric slot loop based connected array MIMO antenna system for 4G/5G terminals," *IEEE Trans. Antennas Propag.*, vol. 65, no. 12, pp. 6679–6686, Feb. 2017.
[6] Y. Yang, R. S. Blum, and S. Sfar, "Antenna selection for MIMO systems with closely spaced antennas," *EURASIP J. Wireless Commun. Netw.*, vol. 2009, no. 1, pp. 1–11, Dec. 2009.
[7] Y.-L. Ban, C. Li, C.-Y.-D. Sim, G. Wu, and K.-L. Wong, "4G/5G multiple antennas for future multi-mode smartphone applications," *IEEE Access*, vol. 4, pp. 2981–2988, 2016.
[8] X. Shi, M. Zhang, S. Xu, D. Liu, H. Wen, and J. Wang, "Dual-band 8-element MIMO antenna with short neutral line for 5G mobile handset," in *Proc. 11th Eur. Conf. Antennas Propag. (EUCAP)*, Mar. 2017, pp. 3140–3142.
[9] W. Jiang, B. Liu, Y. Cui, and W. Hu, "High-isolation eight-element MIMO array for 5G smartphone applications," *IEEE Access*, vol. 7, pp. 34104–34112, 2019.
[10] M. Abdullah, S. H. Kiani, and A. Iqbal, "Eight element multiple-input multiple-output (MIMO) antenna for 5G mobile applications," *IEEE Access*, vol. 7, pp. 134488–134495, 2019.
[11] K.-L. Wong and J.-Y. Lu, "3.6-GHz 10-antenna array for MIMO operation in the smartphone," *Microw. Opt. Technol. Lett.*, vol. 57, no. 7, pp. 1699–1704, Jul. 2015.
[12] J.-Y. Deng, J. Yao, D.-Q. Sun, and L.-X. Guo, "Ten-element MIMO antenna for 5G terminals," *Microw. Opt. Technol. Lett.*, vol. 60, no. 12, pp. 3045–3049, Dec. 2018.
[13] W. Hu, X. Liu, S. Gao, L.-H. Wen, L. Qian, T. Feng, R. Xu, P. Fei, and Y. Liu, "Dual-band ten-element MIMO array based on dual-mode IFAs for 5G terminal applications," *IEEE Access*, vol. 7, pp. 178476–178485, 2019.
[14] M.-Y. Li, Y.-L. Ban, Z.-Q. Xu, J. Guo, and Z.-F. Yu, "Tri-polarized 12-antenna MIMO array for future 5G smartphone applications," *IEEE Access*, vol. 6, pp. 6160–6170, 2018.
[15] H. Wang and G. Yang, "Compact side-edge frame printed fourteen-element antenna array for triple-band MIMO operations in the 5G smartphone," in *Proc. Int. Conf. Microw. Millim. Wave Technol. (ICMMT)*, May 2019, pp. 1–3.
[16] K.-L. Wong, J.-Y. Lu, L.-Y. Chen, W.-Y. Li, and Y.-L. Ban, "8-antenna and 16-antenna arrays using the quad-antenna linear array as a building block for the 3.5-GHz LTE MIMO operation in the smartphone," *Microw. Opt. Technol. Lett.*, vol. 58, no. 1, pp. 174–181, Jan. 2016.
[17] C.-Y. Tsai, K.-L. Wong, and W.-Y. Li, "Experimental results of the multi-gbps smartphone with 20 multi-input multi-output (MIMO) antennas in the 20 × 12 MIMO operation," *Microw. Opt. Technol. Lett.*, vol. 60, no. 8, pp. 2001–2010, Aug. 2018.
[18] K. Zhao, Z. Ying, S. Zhang, and G. Pedersen, "User body effects on mobile antennas and wireless systems of 5G communication," in *Proc. 14th Eur. Conf. Antennas Propag. (EuCAP)*, Mar. 2020, pp. 1–5.
[19] K. Zhao, C. Gustafson, Q. Liao, S. Zhang, T. Bolin, Z. Ying, and S. He, "Channel characteristics and user body effects in an outdoor urban scenario at 15 and 28 GHz," *IEEE Trans. Antennas Propag.*, vol. 65, no. 12, pp. 6534–6548, Dec. 2017.

[20] B. Xu, Z. Ying, L. Scialacqua, A. Scannavini, L. J. Foged, T. Bolin, K. Zhao, S. He, and M. Gustafsson, "Radiation performance analysis of 28 GHz antennas integrated in 5G mobile terminal housing," *IEEE Access*, vol. 6, pp. 48088–48101, 2018.
[21] T. Q. K. Nguyen, M. S. Miah, L. Lizzi, K. Haneda, and F. Ferrero, "Experimental evaluation of user's finger effects on a 5G terminal antenna array at 26 GHz," *IEEE Antennas Wireless Propag. Lett.*, vol. 19, no. 6, pp. 892–896, Jun. 2020.
[22] Q. Wu, J. Huang, J. Liu, Q. Yue, Z. Ding, and Z. Liu, "A compact 12-port MIMO mobile antenna with dual LTE band," in *Proc. Int. Appl. Comput. Electromagn. Soc. Symp.-China (ACES)*, Aug. 2019, pp. 1–2.
[23] J. Lee, H.-H. Hsu, and Y.-E. Ho, "Scalable package-level RFI filter for digital clock noise mitigation in 5-GHz and future 6-GHz WiFi applications," in *Proc. IEEE Int. Symp. Electromagn. Compat., Signal Power Integrity (EMC+SIPI)*, Jul. 2019, pp. 427–431.
[24] G. Ahmed, S. U. Islam, M. Shahid, A. Akhunzada, S. Jabbar, M. K. Khan, M. Riaz, and K. Han, "Rigorous analysis and evaluation of specific absorption rate (SAR) for mobile multimedia healthcare," *IEEE Access*, vol. 6, pp. 29602–29610, 2018.
[25] H. H. Zhang, G. G. Yu, Y. Liu, Y. X. Fang, G. Shi, and S. Wang, "Design of low-SAR mobile phone antenna: Theory and applications," *IEEE Trans. Antennas Propag.*, vol. 69, no. 2, pp. 698–707, Feb. 2021.
[26] M. S. Sharawi, "Current misuses and future prospects for printed multiple-input, multiple-output antenna systems," *IEEE Antenna Propag Mag.*, vol. 59, no. 2, pp. 162–170, Apr. 2017.
[27] L. Song and J. Shen, *Evolved Cellular Network Planning and Optimization for UMTS and LTE*. Boca Raton, FL, USA: CRC Press, 2010.
[28] M. S. Sharawi, "Printed multi-band MIMO antenna systems and their performance metrics [wireless corner]," *IEEE Antennas Propag. Mag.*, vol. 55, no. 5, pp. 218–232, Oct. 2013.
[29] A. M. Elshirkasi, A. A. Al-Hadi, M. F. Mansor, R. Khan, and P. J. Soh, "Envelope correlation coefficient of a two-port MIMO terminal antenna under uniform and Gaussian angular power spectrum with user's hand effect," *Prog. Electromagn. Res. C*, vol. 92, pp. 123–136, 2019.
[30] K. Zhao, E. Bengtsson, Z. Ying, and S. He, "Multiplexing efficiency of high order MIMO in mobile terminal in different propagation scenarios," in *Proc. 10th Eur. Conf. Antennas Propag. (EuCAP)*, Apr. 2016, pp. 1–4.
[31] R. Tian, B. K. Lau, and Z. Ying, "Multiplexing efficiency of MIMO antennas," *IEEE Antennas Wireless Propag. Lett.*, vol. 10, pp. 183–186, 2011.
[32] R. Tian, B. K. Lau, and Z. Ying, "Multiplexing efficiency of MIMO antennas with user effects," in *Proc. IEEE Int. Symp. Antennas Propag. (APSURSI)*, Jul. 2012, pp. 1–2.
[33] Z. Ying, K. Zhao, T. Bolin, S. He, A. Scannavini, L. J. Foged, and G. Nicolas, "Multiplexing efficiency of high order MIMO in mobile terminal for 5G communication at 15 GHz," in *Proc. Int. Symp. Antennas Propag. (ISAP)*, 2016, pp. 594–595.
[34] X. Chen, J. Tang, S. Zhu, and A. Zhang, "Characterizations of MIMO antennas using multiplexing efficiency," in *Proc. IEEE Int. Symp. Antennas Propag., USNC/URSI Nat. Radio Sci. Meeting*, Jul. 2018, pp. 375–376.
[35] X. Chen, "Antenna correlation and its impact on multi-antenna system," *Prog. Electromagn. Res. B*, vol. 62, pp. 241–253, 2015.
[36] A. Goldsmith, *Wireless Communications*. Cambridge, U.K.: Cambridge Univ. Press, 2005.
[37] I. Vasilev, V. Plicanic, and B. K. Lau, "Impact of antenna design on MIMO performance for compact terminals with adaptive impedance matching," *IEEE Trans. Antennas Propag.*, vol. 64, no. 4, pp. 1454–1465, Apr. 2016.
[38] A. Zhao and Z. Ren, "Wideband MIMO antenna systems based on coupled-loop antenna for 5G N77/N78/N79 applications in mobile terminals," *IEEE Access*, vol. 7, pp. 93761–93771, 2019.
[39] M. Abdullah, S. H. Kiani, L. F. Abdulrazak, A. Iqbal, M. A. Bashir, S. Khan, and S. Kim, "High-performance multiple-input multiple-output antenna system for 5G mobile terminals," *Electronics*, vol. 8, no. 10, p. 1090, Sep. 2019.
[40] J. L. Guo, L. Cui, C. Li, and B. H. Sun, "Side-edge frame printed eight-port dual-band antenna array for 5G smartphone applications," *IEEE Trans. Antennas Propag.*, vol. 66, no. 12, pp. 7412–7417, Dec. 2018.
[41] Y. Li, C.-Y.-D. Sim, Y. Luo, and G. Yang, "Multiband 10-antenna array for sub-6 GHz MIMO applications in 5-G smartphones," *IEEE Access*, vol. 6, pp. 28041–28053, 2018.
[42] A. M. Elshirkasi, A. A. Al-Hadi, P. J. Soh, M. F. Mansor, R. Khan, X. Chen, and P. Akkaraekthalin, "Performance study of a MIMO mobile terminal with upto 18 elements operating in the sub-6 GHz 5G band with user hand," *IEEE Access*, vol. 8, pp. 28164–28177, 2020.
[43] N. Jaglan, S. D. Gupta, and M. S. Sharawi, "18 element massive MIMO/diversity 5G smartphones antenna design for sub-6 GHz LTE bands 42/43 applications," *IEEE Open J. Antennas Propag.*, vol. 2, pp. 533–545, 2021.
[44] C. Ouyang and H. Yang, "Massive MIMO antenna selection: Asymptotic upper capacity bound and partial CSI," 2018, *arXiv:1812.06595*.
[45] W. An, P. Zhang, J. Xu, H. Luo, L. Huang, and S. Zhong, "A novel machine learning aided antenna selection scheme for MIMO Internet of Things," *Sensors*, vol. 20, no. 8, p. 2250, Apr. 2020.
[46] A. S. Hiwale and A. A. Ghatol, "A reduced complexity MIMO system with antenna selection for high-data rate wireless communications," *J. Sci. Ind. Res.*, vol. 7, pp. 498–504, Jul. 2007.

AHMED MOHAMED ELSHIRKASI received the M.Sc. degree in communication engineering from International Islamic University Malaysia (IIUM), in 2015, and the Ph.D. degree from the Universiti Malaysia Perlis (UniMAP), in 2021. His current research interests include the performance evaluation of MIMO antennas, mobile terminal antennas and their user interactions, and wireless propagation.

AZREMI ABDULLAH AL-HADI (Senior Member, IEEE) received the Master of Science degree in communication engineering from Birmingham University, U.K., in 2004, and the Doctor of Science in Technology degree from Aalto University, Finland, in 2013.

Since 2002, he has been with the Universiti Malaysia Perlis (UniMAP). He is currently working as an Associate Professor and the Dean of the Faculty of Electronic Engineering Technology, UniMAP. His current research interests include design and performance evaluation of multi-element antennas, mobile terminal antennas and their user interactions, and wireless propagation.

Dr. Azremi is a member of the Board of Engineers Malaysia (BEM), Malaysia. He was a recipient of the Best Student Paper Award presented at the 5th Loughborough Antennas and Propagation Conference (LAPC 2009), the CST University Publication Award in 2011, and the Excellence and Best Paper Awards from IEEE Malaysia AP/MTT/EMC Joint Chapter in 2018, 2019, and 2020. During his appointment as the Vice Chair of the IEEE Malaysia AP/MTT/EMC Joint Chapter, the chapter has won the 2020 Outstanding Chapter Award by the IEEE Antennas and Propagation Society. He is active in volunteering work with IEEE Malaysia Section, acting as the Chair of the IEEE Malaysia Antenna Propagation/Microwave Theory Techniques/Electromagnetic Compatibility (AP/MTT/EMC) Joint Chapter and a Past Counselor of the IEEE UniMAP Student Branch. He is the Chartered Engineer of the Institution of Engineering and Technology (IET), U.K., and the Professional Technologist of the Malaysia Board of Technologist (MBOT), Malaysia.

RIZWAN KHAN was born in Abbottabad, Pakistan, in 1990. He received the M.S. degree in electrical engineering from the COMSATS Institute of Information Technology, Abbottabad, in 2015, and the Doctor of Science degree in communication engineering from the Universiti Malaysia Perlis (UniMAP), Malaysia, in 2018. From 2015 to 2016, he worked as a Research Associate with the Department of Electrical Engineering, COMSATS. He is currently working as a RF Engineer at Laird Technologies (M) Sdn Bhd, Penang, Malaysia, and also involves in research at Advanced Communication Engineering (ACE), UniMAP. He has published several impact factors journals, national, and international conference papers. His research interests include mobile terminal antennas and their user interactions, MIMO antennas, dielectric resonator antennas, metamaterial, electrically small antenna, and reconfigurable antennas.

PRAYOOT AKKARAEKTHALIN (Member, IEEE) received the B.Eng. and M.Eng. degrees in electrical engineering from the King Mongkut's University of Technology North Bangkok (KMUTNB), Bangkok, Thailand, in 1986 and 1990, respectively, and the Ph.D. degree from the University of Delaware, Newark, DE, USA, in 1998. From 1986 to 1988, he was a Research and Development Engineer with Microtek Company Ltd., Thailand. In 1988, he joined the Department of Electrical Engineering, KMUTNB. He is also the Leader of TRF Senior Research Scholar Project of "Innovative Sensor Technology for Thailand Development" granted by the Thailand Research Fund, Thailand. He has authored or coauthored over 40 international journals, more than 200 conference papers, and four books/book chapters. His current research interests include RF/microwave circuits, wideband and multiband antennas, telecommunications, and sensor systems. He is a member of the IEICE Japan, ECTI, and EEAAT Associations Thailand. He was the Chairperson of the IEEE MTT/AP/ED Thailand Joint Chapter, from 2007 to 2010, and the Vice President and the President of the ECTI Association, Thailand, from 2012 to 2013 and from 2014 to 2015, respectively. He was the Editor-in-Chief of the *ECTI Transactions*, from 2011 to 2013.

HAITHAM S. BEN ABDELMULA received the B.Sc. degree in computer engineering from the Department of Computer Engineering, University of Tripoli, Libya, in 2006, the M.Sc. degree from the Department of Electrical and Electronics Engineering, University of Kebangsaan Malaysia (UKM), in 2009, and the Ph.D. degree from the School of Computer and Communication Engineering, University Malaysia Perlis (UniMAP), in 2019. He is currently a Lecturer with the College of Computer Technology Zawia. His research interests include optimization algorithms, network security, routing protocol for ad hoc networks, and radio resource management for mobile networks.

AHMED M. BELGHASEM received the M.Sc. degree from the Department of Electrical and Electronics Engineering, University of Kebangsaan Malaysia (UKM), in 2010. He is currently a Lecturer with the College of Renewable Energies Tajoura. His research interests include mobile communication, and computer networks, specifically in LTE, MIMO, and SDN.

AKRAM H. JEBRIL received the B.Sc. degree (Hons.) in communication engineering from the Technical College of Civil Aviation & Meteorology, Tripoli, Libya. He is currently pursuing the Ph.D. degree with the Faculty of Engineering, School of Electrical Engineering, Universiti Teknologi Malaysia (UTM). He worked as a Teaching Assistant for more than two years at the Technical College of Civil Aviation & Meteorology, where he graduated from and had involved in both sides administrative and scientific. He was in charge of the electrical and electronic laboratories with the Department of Communications Engineering. His research interests include low power wide area networks (LPWAN), wireless sensors networks (WSN), and the Internet of Things (IoT). Based on his distinguish graduation, he has been granted a scholarship for postgraduate study abroad (master's and Ph.D.) that is sponsored by the Ministry of Education in Libya, as a plan to increase his scientific attainment and improve his research skills.

PING JACK SOH (Senior Member, IEEE) received the bachelor's and master's degrees from the Universiti Teknologi Malaysia, and the Ph.D. degree from KU Leuven, Belgium.

He is currently an Associate Professor with the Centre for Wireless Communications (CWC), University of Oulu, Finland. He started his career as a Test Engineer (2002–2004) and a Research and Development Engineer (2005–2006). He then joined Universiti Malaysia Perlis (UniMAP), as a Lecturer, (2006–2009), before moving to the KU Leuven, as a Research Assistant (2009–2013), a Postdoctoral Research Fellow (2013–2014), and since 2014, a Research Affiliate with the ESAT-WAVECORE Research Division. He went back to UniMAP as a Senior Lecturer (2014–2017) and an Associate Professor (2017–2021), before moving to Finland. Within UniMAP, he was formerly the Deputy Director of the Centre for Industrial Collaboration (2007–2009), the Deputy Dean of the university's Research Management and Innovation Center (RMIC) (2014–2017), and the Head of the Advanced Communication Engineering (ACE) Research Centre (2020). His research interests include antennas and related technologies; focused on their applications in wearables/body area communication; compact satellites; metasurfaces; 5G/6G communications; EM safety and absorption; and wireless techniques for healthcare.

Dr. Soh is a member of the IET and URSI. He was a recipient of the URSI Young Scientist Award in 2015, the IEEE MTT-S Graduate Fellowship for Medical Applications in 2013, and the IEEE AP-S Doctoral Research Award in 2012. He was also the Second Place Winner of the IEEE Presidents' Change the World Competition in 2013. Three of his (co)authored journals were awarded the IEEE Malaysia AP/MTT/EMC Joint Chapter's Publication Award in 2020, 2019, and 2018, and another two journals were also awarded the CST University Publication Award in 2012 and 2011. He is a Chartered Engineer registered with the U.K. Engineering Council. He also volunteers in the IEEE MTT-S Education Committee. He is also an Associate Editor of the *International Journal of Numerical Modelling: Electronic Networks, Devices and Fields* (Wiley).